PHYSICAL REVIEW D **79,** 103006 (2009)

Stable configurations of hybrid stars with color-flavor-locked core

B. K. Agrawal[1,*] and Shashi K. Dhiman[2,3,†]

[1]*Saha Institute of Nuclear Physics, Kolkata 700064, India*

[2]*Department of Physics, Himachal Pradesh University, Shimla 171005, India*

[3]*University Institute of Information Technology, Himachal Pradesh University, Shimla 171005, India*

(Received 2 January 2009; published 13 May 2009)

We construct static and mass-shedding limit sequences of hybrid stars, composed of a color flavour locked (CFL) quark matter core, for a set of equations of state (EOSs). The EOS for the hadronic matter is obtained using an appropriately calibrated, extended field theoretical based, relativistic mean-field model. The MIT bag model is employed to compute the EOSs of the CFL quark matter for different values of the CFL gap parameter in the range of 50–150 MeV with the deconfinement phase transition density ranging from $4\rho_0$ to $6\rho_0$ ($\rho_0 = 0.16$ fm^{-3}). We find that, depending on the values of the CFL gap parameter and the deconfinement phase transition density, the sequences of stable configurations of hybrid stars either form third families of the compact stars or bifurcate from the hadronic sequence. The hybrid stars have masses 1.0–2.1$M_\odot$ with radii 9–13.5 km. The maximum values of the mass-shedding limit frequency for such hybrid stars are 1–2 kHz. For the smaller values of the CFL gap parameter and the deconfinement phase transition density, mass-radius relationships are in harmony with those deduced by applying an improved hydrogen atmosphere model to fit the high quality spectra from compact star X7 in the globular cluster 47 Tucanae. We observed, for some cases, that the third family of compact stars exist in the static sequence but disappear from the mass-shedding limit sequence. Our investigation suggests that the third family of compact stars in the mass-shedding limit sequence is more likely to appear, provided these stars have maximum mass in the static limit higher than their second-family counterpart composed of pure hadronic matter.

DOI: 10.1103/PhysRevD.79.103006 PACS numbers: 97.60.Jd, 12.38.−t, 26.60.Kp

I. INTRODUCTION

The suggestion that three-flavor quark matter may be the ground state of strongly interacting systems [1–3] led to the postulation that quark stars are possible astrophysical objects. It was also hypothesized that some compact stars might be hybrid stars with a core composed of quark matter and surrounded by a nuclear mantle. The present knowledge of quantum chromodynamics (QCD) at high density indicates that quark matter might be in a color superconducting phase. The essence of color superconductivity is the quark-quark color superconductor [4,5] and is driven by the Bardeen, Cooper, and Schrieffer (BCS) [6,7] pairing mechanism. The possible quark color superconducting phases include the two-flavor color superconductor (2SC) [8–10], the color-flavor-locked (CFL) phase [11,12], and the crystalline color superconductor (CCS) [13–15]. The speculation that color superconducting quark matter is present in the core of the hybrid stars has triggered many theoretical investigations.

The hybrid stars with a CFL quark matter core have been extensively studied. The hadron phase of the hybrid star matter is described by various models which can be broadly grouped into (i) nonrelativistic potential models [16], (ii) nonrelativistic mean-field models [17–20], (iii) field theoretical based relativistic mean-field models (FTRMF) [21–23], and the (iv) Dirac-Brueckner-Hartree-Fock model [24–27]. The CFL quark matter appearing at the core of hybrid stars is described within the MIT bag model and the Nambu-Jona-Lasinio (NJL) model. The studies based on the MIT bag model indicate the existence of stable configurations of hybrid stars with a CFL quark matter core [28–30]. Two different situations are encountered: the hybrid stars with a CFL quark matter core either form a third family of compact stars separated from the purely hadronic sequence by an instability region, or bifurcate from the hadronic sequence of stars when the central density exceeds the phase transition density at which deconfinement of hadrons to CFL quark matter occurs. The scenario is completely different when the NJL model is employed to study the hybrid stars with a CFL quark matter core. Until recently [31–33], it was shown that the NJL-like model rules out the CFL quark matter phase at the core because it renders the hybrid star unstable. Only very recently has it been found that large enough values of the diquark coupling strength in the NJL model can yield stable configurations of a hybrid star containing a CFL quark matter core [34,35].

The stability of the hybrid star with a CFL quark matter core depends strongly on the values of the deconfinement phase transition density and the CFL gap parameter, which are poorly known. In the present work we construct the static sequences of hybrid stars, with a CFL quark matter

*bijay.agrawal@saha.ac.in

†shashi.dhiman@gmail.com

core, for a set of equations of state (EOSs) obtained for different values of the CFL gap parameter and the deconfinement phase transition density. The hadron phase of the hybrid star is described by using an appropriately calibrated extended FTRMF model which includes the contributions from self-interaction and mixed interaction terms for σ, ω, and ρ mesons up to the quartic order. The CFL quark matter phase is described within the MIT bag model with an additional parameter that mimics the effect of including perturbative QCD corrections. Instead of keeping the value of the bag constant as previously done [28,29], calculations are performed for different values of the CFL gap parameter at fixed values of the deconfinement phase transition density. This strategy should enable us to better assess the influence of the CFL gap parameter on the properties of hybrid stars with a CFL quark matter core. The CFL gap parameter Δ is varied in the range of 50–150 MeV by keeping the deconfinement phase transition density ρ_t fixed in between $4\rho_0$ and $6\rho_0$ ($\rho_0 = 0.16$ fm^{-3}). For the different values of the CFL gap parameter considered, the average quark chemical potential at the deconfinement phase transition density lies in the range of 375–500 MeV, which is in reasonable agreement with the predictions of the NJL model.

The paper is organized as follows. In Sec. II we describe, in brief, the models used to construct the EOSs for the hadronic phase, the CFL quark phase, and the mixed phase. In Sec. III we present the results for static and mass-shedding limit sequences for hybrid stars. In Sec. IV we state our conclusions.

II. EQUATIONS OF STATE FOR HYBRID STAR MATTER

We construct the EOS for hybrid star matter, which is composed of hadrons at low densities, quark matter in the CFL phase at high densities, and the mixed phase at intermediate densities. The EOS for hadron matter is obtained within the framework of the extended FTRMF model. The EOS for quark matter in the CFL phase is obtained using the MIT bag model. The EOS for the mixed phase is constructed using the Gibbs conditions. For the hadron matter at very low densities, $\rho \sim 0.5\rho_0$ fm^{-3} going down to $\rho = 6.0 \times 10^{-12}$ fm^{-3}, we use Negele-Vautherin [36] and Baym-Pethick-Sutherland EOSs [37].

A. Hadron phase

The hadronic phase is described using the extended FTRMF model, which includes the contributions from self-interaction and mixed interaction terms for σ, ω, and ρ mesons up to the quartic order. The mixed interaction terms involving the ρ-meson field enable one to vary the density dependence of the symmetry energy coefficient and neutron-skin thickness in heavy nuclei over a wide range without affecting the other properties of the finite nuclei [38,39]. The contribution from the self-interaction of ω mesons plays an important role in determining the high density behavior of the EOS and, consequently, the structure properties of compact stars [40,41]. The contributions of self-interactions of ρ mesons are ignored, as they affect the ground state properties of heavy nuclei and compact stars only very marginally [41]. In our recent work [40] we have obtained several parametrizations of the extended FTRMF model in such a way that the bulk nuclear observables and nuclear matter incompressibility coefficient are fitted well. These different parametrizations produce different behaviors for the EOSs at high densities.

The energy density of the hadron phase in the extended FTRMF models is given by

$$\begin{aligned}\mathcal{E}_{\rm HP}(\mu_n,\mu_e) &= \frac{1}{\pi^2}\sum_{j=n,p}\int_0^{k_f^j} k^2\sqrt{k^2+M^{*2}}dk + g_{\omega N}\omega(\rho_p+\rho_n) + \frac{1}{2}g_{\rho N}\rho(\rho_p-\rho_n) + \frac{1}{2}m_\sigma^2\sigma^2 + \frac{\bar\kappa}{6}g_{\sigma N}^3\sigma^3 + \frac{\bar\lambda}{24}g_{\sigma N}^4\sigma^4 \\ &- \frac{\zeta}{24}g_{\omega N}^4\omega^4 - \frac{1}{2}m_\omega^2\omega^2 - \frac{1}{2}m_\rho^2\tilde\rho^2 - \bar\alpha_1 g_{\sigma N}g_{\omega N}^2\sigma\omega^2 - \frac{1}{2}\bar\alpha_1' g_{\sigma N}^2 g_{\omega N}^2\sigma^2\omega^2 - \bar\alpha_2 g_{\sigma N}g_{\rho N}^2\sigma\rho^2 \\ &- \frac{1}{2}\bar\alpha_2' g_{\sigma N}^2 g_{\rho N}^2\sigma^2\rho^2 - \frac{1}{2}\bar\alpha_3' g_{\omega N}^2 g_{\rho N}^2\omega^2\rho^2 + \frac{1}{\pi^2}\sum_{l=e^-,\mu^-}\int_0^{k_f^l} k^2\sqrt{k^2+m_l^2}dk. \end{aligned} \tag{1}$$

The pressure of the hadron phase matter is given by

$$\begin{aligned}P_{\rm HP}(\mu_n,\mu_e) &= \frac{1}{3\pi^2}\sum_{j=n,p}\int_0^{k_f^j}\frac{k^4dk}{\sqrt{k^2+M^{*2}}} - \frac{1}{2}m_\sigma^2\sigma^2 - \frac{\bar\kappa}{6}g_{\sigma N}^3\sigma^3 - \frac{\bar\lambda}{24}g_{\sigma N}^4\sigma^4 + \frac{\zeta}{24}g_{\omega N}^4\omega^4 + \frac{1}{2}m_\omega^2\omega^2 + \frac{1}{2}m_\rho^2\rho^2 \\ &+ \bar\alpha_1 g_{\sigma N}g_{\omega N}^2\sigma\omega^2 + \frac{1}{2}\bar\alpha_1' g_{\sigma N}^2 g_{\omega N}^2\sigma^2\omega^2 + \bar\alpha_2 g_{\sigma N}g_{\rho N}^2\sigma\rho^2 + \frac{1}{2}\bar\alpha_2' g_{\sigma N}^2 g_{\rho N}^2\sigma^2\rho^2 + \frac{1}{2}\bar\alpha_3' g_{\omega N}^2 g_{\rho N}^2\omega^2\rho^2 \\ &+ \frac{1}{3\pi^2}\sum_{l=e^-,\mu^-}\int_0^{k_f^l}\frac{k^4dk}{\sqrt{k^2+m_l^2}}, \end{aligned} \tag{2}$$

where $M^* = M - g_{\sigma N}\sigma$ is the effective mass of the nucleon, with M being the free nucleon mass. In Eqs. (1) and (2), σ, ω, and ρ represent the meson fields. The $g_{\sigma N}$, $g_{\omega N}$, and $g_{\rho N}$ are the meson-nucleon coupling strengths. The m_σ, m_ω, and m_ρ are the masses for the σ, ω, and ρ mesons. The coupling strengths for the self-interaction terms for the σ and ω mesons are denoted by $\bar{k}$, $\bar{\lambda}$, and $\bar{\zeta}$. The constants $\bar{\alpha}$ and $\bar{\alpha}'$ represent the coupling strengths for various mixed interaction terms. The last terms in Eqs. (1) and (2) give the contributions to the energy density and pressure from leptons, respectively. In Eqs. (1) and (2), μ_n and μ_e represent the chemical potentials for the neutrons and electrons, respectively. The chemical potentials for the protons μ_p and the muons μ_μ can be expressed in terms of μ_n and μ_e using the β-equilibrium conditions, i.e.,

$$\mu_n = \mu_p + \mu_e, \tag{3}$$

$$\mu_e = \mu_\mu. \tag{4}$$

Once the chemical potentials for the nucleons are known, their Fermi momenta can be obtained by solving the field equations for the mesons as given in Ref. [40]. The Fermi momenta k_f^l for the leptons are obtained as

$$k_f^l = \sqrt{\mu_l^2 - m_l^2}. \tag{5}$$

In addition to the conditions of the β equilibrium, matter in the pure hadronic phase is considered to be charge neutral.

B. Quark matter in the CFL phase

The free energy density for quark matter in the CFL phase is taken to be [42]

$$\Omega_{\rm CFL}(\mu, \mu_e) = \Omega_{\rm CFL}^{\rm quarks}(\mu) + \Omega_{\rm CFL}^{\rm GB}(\mu, \mu_e) + \Omega^{\rm electron}(\mu_e), \tag{6}$$

where μ is the average chemical potential for quarks and μ_e is the electron chemical potential. The contribution to Eq. (6) from the quarks is given by

$$\Omega_{\rm CFL}^{\rm quarks} = \frac{6}{\pi^2}\int_0^\nu p^2(p-\mu)dp + \frac{3}{\pi^2} \times \int_0^\nu p^2\left(\sqrt{p^2+m_s^2} - \mu\right)dp + \frac{3}{4\pi^2}c\mu^4 - \frac{3\Delta^2\mu^2}{\pi^2} + B, \tag{7}$$

where u and d quarks are assumed to be massless and the s quark has the mass m_s. The term proportional to μ^4 in Eq. (7) corresponds to the QCD inspired correction [43]. The second to last term involving the CFL gap parameter Δ is the lowest order contribution from the formation of the CFL condensate. The last term B is the bag model constant, which accounts for the energy difference between the perturbative vacuum and the true vacuum. The number densities for all three flavors of quarks considered are the same and can be obtained as

$$\rho_q = \frac{1}{\pi^2}(\nu^3 - c\mu^3 + 2\Delta^2\mu) \tag{8}$$

with $q = u$, d, and s, and the common Fermi momentum ν given as

$$\nu = 2\mu - \sqrt{\mu^2 + \frac{m_s^2}{3}}. \tag{9}$$

The contribution to Eq. (6) from the Goldstone bosons arising due to the breaking of chiral symmetry in the CFL phase is evaluated using $\Omega_{\rm CFL}^{\rm GB}(\mu, \mu_e)$ [44],

$$\Omega_{\rm CFL}^{\rm GB}(\mu, \mu_e) = -\frac{1}{2}f_\pi^2\mu_e^2\left(1 - \frac{m_{\pi^-}^2}{\mu_e^2}\right)^2 \tag{10}$$

where the parameters are

$$f_\pi^2 = \frac{(21 - 8\ln 2)\mu^2}{36\pi^2}, \qquad m_{\pi^-}^2 = \frac{3\Delta^2}{\pi^2 f_\pi^2}m_s(m_u + m_d), \tag{11}$$

$$\Omega^{\rm lepton}(\mu_e) = \frac{1}{\pi^2}\sum_{i=e^-,\mu^-}\int_0^{\sqrt{\mu_e^2 - m_i^2}} p^2\left(\sqrt{p^2+m_i^2} - \mu_e\right)dp. \tag{12}$$

The total energy density and pressure for the quark phase can be calculated as

$$\mathcal{E}_{\rm QP} = \Omega_{\rm CFL}(\mu, \mu_e) + 3\mu\rho_q + \mu_e(\rho_e + \rho_\mu) \tag{13}$$

and

$$P_{\rm QP} = -\Omega_{\rm CFL}(\mu, \mu_e). \tag{14}$$

It is clear from Eq. (8) that the densities for the u, d, and s quarks are equal to each other for quark matter in the CFL phase. Thus, quark matter in the CFL phase is enforced to be charge neutral. The electrons are present only in the mixed phase of hadronic and quark matter.

C. Mixed phase

The EOS for the mixed phase composed of hadronic and CFL quark matter is obtained using the Gibbs conditions. The Gibbs conditions can be expressed in terms of two independent chemical potentials, in our case, as

$$P_{\rm HP}(\mu_n, \mu_e) = P_{\rm QP}(\mu, \mu_e) \tag{15}$$

where μ_n and μ_e are the two independent chemical potentials, with μ_n being the neutron chemical potential. In the mixed phase the average quark chemical potential $\mu = \mu_n/3$, and the local charge neutrality condition is replaced by the global charge neutrality

$$\chi\rho_{\rm QP}^{\rm ch} + (1-\chi)\rho_{\rm HP}^{\rm ch} = 0, \tag{16}$$

where χ is the volume fraction occupied by quark matter in the mixed phase and $\rho^{\rm ch}$ is the charge density. It is clear from Eq. (16) that both hadron and quark matter are allowed to be charged separately. The energy density $\mathcal{E}_{\rm MP}$ and the hadron density $\rho_{\rm MP}$ of the mixed phase can be calculated as [45]

$$\mathcal{E}_{\rm MP} = \chi\mathcal{E}_{\rm QP} + (1-\chi)\mathcal{E}_{\rm HP}, \tag{17}$$

$$\rho_{\rm MP} = \chi\rho_{\rm QP} + (1-\chi)\rho_{\rm HP}. \tag{18}$$

Once these quantities are determined, we can construct the complete EOS with the hadron phase, the quark matter phase, and the mixed phase, and compute the properties of hybrid compact stars.

III. STRUCTURE OF HYBRID STARS WITH CFL CORE

We study the properties of the hybrid stars, composed of a CFL quark matter core, for a set of EOSs obtained for different values of the CFL gap parameter Δ and the deconfinement phase transition density ρ_t. Instead of using fixed values of the bag constant as is customarily done [28,29,46], we adjust the bag constant for each value of the CFL gap parameter to yield the desired value of the phase transition density. We consider the values of the CFL gap parameter in the range of 50–150 MeV as estimated and employed for the studies of hybrid stars [28,35,42,47]. In Fig. 1 we plot several EOSs for hybrid star matter obtained for different values of the CFL gap parameter Δ with $\rho_t = 4\rho_0$–$6\rho_0$. The EOS for the hadron phase is obtained within the framework of the extended FTRMF model as discussed in the preceding section. In Ref. [40] we have obtained several parameter sets for the extended FTRMF model for different values of the coupling strength of the ω-meson self-interaction term and the neutron-skin thickness in the ^{208}Pb nucleus, as these are not well determined from the presently available experimental data. Each of the parametrizations is consistent with bulk properties of the finite nuclei and nuclear matter. In the present work we have employed the parameter set which corresponds to the ω-meson self-interaction strength $\zeta = 0$ [Eq. (1)] and a neutron-skin thickness of 0.2 fm in the ^{208}Pb nucleus. The choice of $\zeta = 0$ yields stiff EOSs for hadronic matter at high densities. The EOSs of CFL quark matter for different values of Δ and ρ_t are obtained using strange quark mass $m_s = 150$ MeV and the constant $c = 0.3$ in Eq. (7). In Fig. 2 we plot the values of the bag constant $B^{1/4}$ as a function of Δ for $\rho_t = 4\rho_0 - 6\rho_0$. We get somewhat higher values of B compared to the ones commonly used. In particular, the value of B increases rapidly with the deconfinement phase transition density. This is because stiffness of the EOS for the hadronic matter considered here increases rapidly with density. Further, as the CFL gap parameter increases, the value of B increases to keep the phase transition density unaltered. In Fig. 3 we plot the values of the average quark chemical potential μ_t at the deconfinement phase transition densities $\rho_t = 4\rho_0$–$6\rho_0$ as a function of the CFL gap parameter. For our choice of the phase transition densities, the values of μ_t are in the range of 375–500 MeV, which is in reasonable agreement with the ones obtained in Refs. [15,34]. The properties of the static and rotating compact stars resulting from our set of

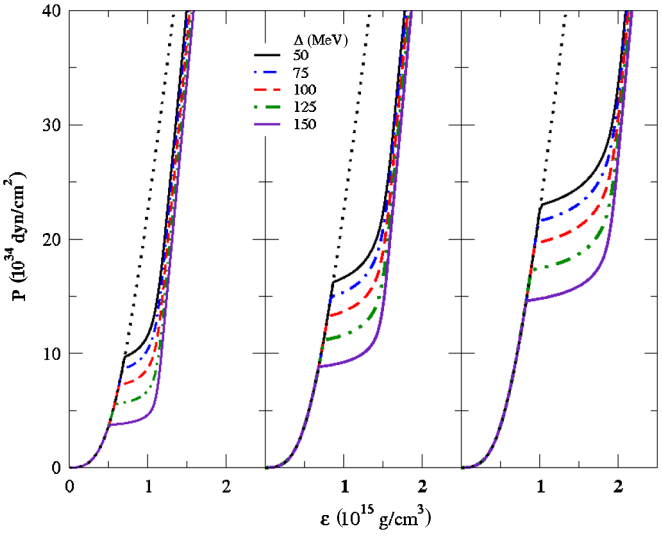

FIG. 1 (color online). Pressure as a function of energy density for different values of the CFL gap parameter with hadron to CFL quark matter phase transition densities $\rho_t = 4\rho_0$ (left), $5\rho_0$ (middle), and $6\rho_0$ (right). The EOS for pure hadronic matter is shown by the black dotted line.

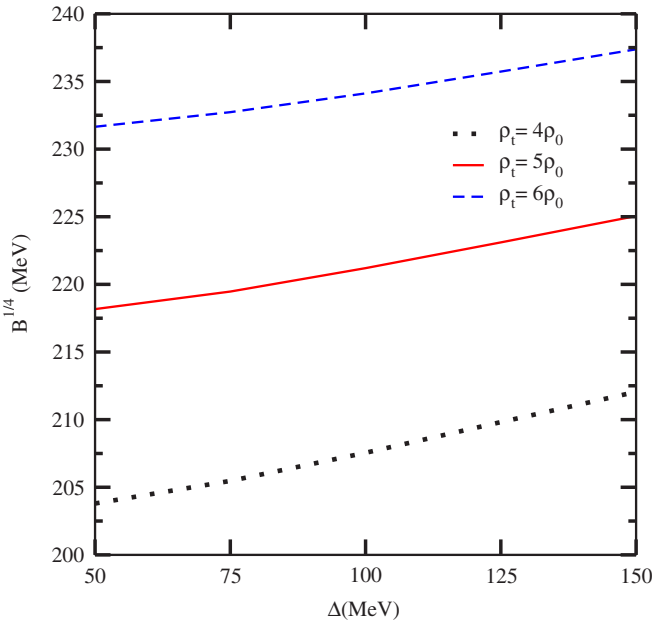

FIG. 2 (color online). Variations of the bag constant as a function of the CFL gap parameter at fixed values of hadron to CFL quark matter phase transition densities $4\rho_0$–$6\rho_0$.

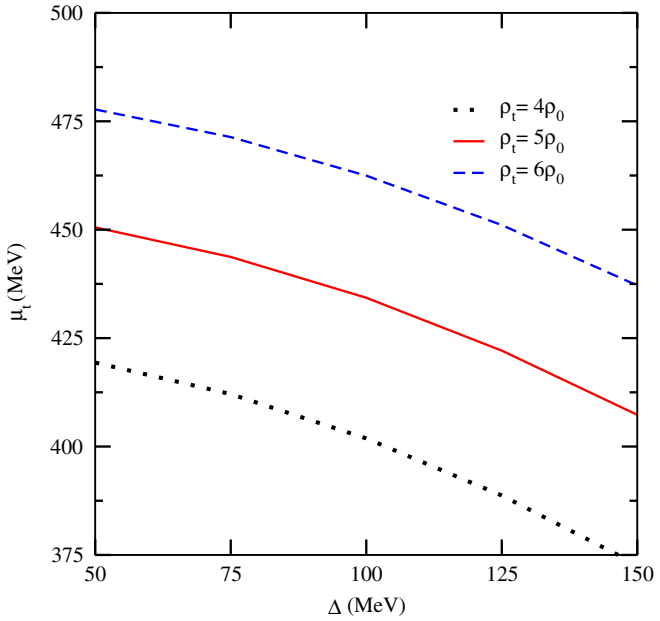

FIG. 3 (color online). Variations of the average value of the quark chemical potential at the phase transition density as a function of the CFL gap parameter.

EOSs are computed using the code developed by Stergioulas [48].

A. Static sequences

The sequence of static compact stars is obtained by varying the central energy density ϵ_c for a given EOS. For a stable configuration,

$$\frac{\partial M}{\partial \epsilon_c} > 0 \tag{19}$$

where M is the gravitational mass of the static compact star. In Figs. 4–6 we plot the mass-radius relationships for static sequences obtained for various EOSs corresponding to the different values of the CFL gap parameter $\Delta =$ 50–150 MeV with $\rho_t = 4\rho_0$–$6\rho_0$. The solid circle on each of the curves marks the point at which the deconfinement phase transition from hadron to CFL quark matter occurs. The curves on the left of the solid circles represent the sequences of the hybrid stars with a CFL quark matter core. The black dotted line represents the static sequence of the compact stars composed of pure hadronic matter. The radius of the hybrid stars decreases with increasing central energy density. It can be seen that the stable configurations of hybrid stars with a CFL quark matter core either bifurcate from the hadronic sequence or form a different branch, the so-called third family of compact stars [45,49]. With $\rho_t = 4\rho_0$–$5\rho_0$, the stable configurations of the hybrid stars exist for all values of the CFL gap parameter considered. In particular, for $\Delta = 50$–100 MeV with $\rho_t = 4\rho_0$, sequences of stable configurations of the hybrid stars bifurcate from the hadronic sequence at the central density, exceed-

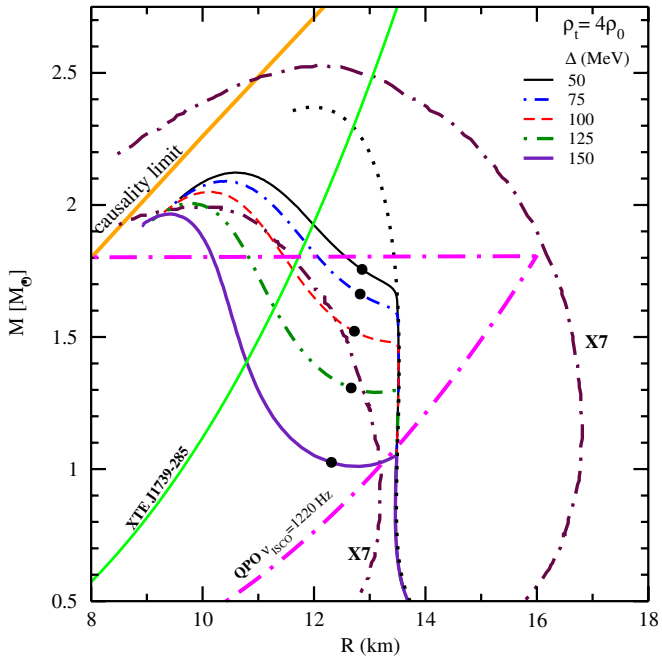

FIG. 4 (color online). Plots for the mass-radius relationships for the static sequences obtained using fixed values of the CFL gap parameter Δ ranging from 50 MeV to 150 MeV with a deconfinement phase transition density $\rho_t = 4\rho_0$. The dotted black line represents the static sequence of compact stars composed of hadronic matter. The solid circle on each of the curves denotes the end of the mixed phase. The curves on the left of the solid circles represent the hybrid stars with a CFL core. The dot-dashed maroon curves are the mass-radius contours deduced with 90% confidence by fitting the high quality spectra from the compact star X7 in the globular cluster 47 Tucanae [50].

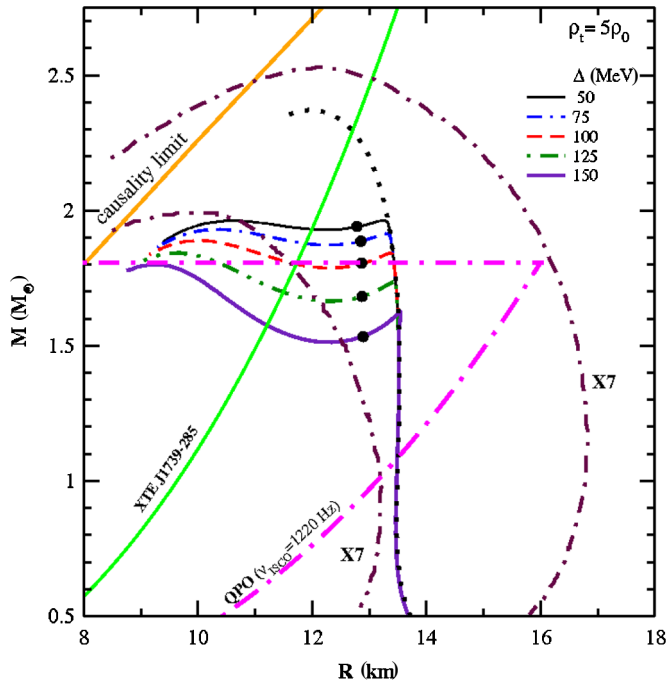

FIG. 5 (color online). Same as Fig. 4, but for the deconfinement phase transition density $\rho_t = 5\rho_0$.

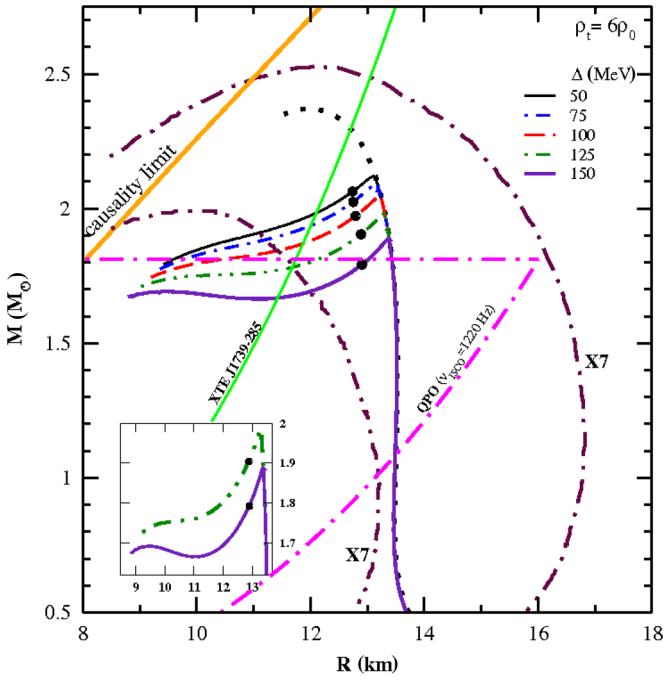

FIG. 6 (color online). Same as Fig. 4, but for the deconfinement phase transition density $\rho_t = 6\rho_0$. The inset highlights the appearance of third families of compact stars for the CFL gap parameter $\Delta \geq 125$ MeV.

ing the one at which the onset of the mixed phase occurs. For all the other cases with $\rho_t = 4\rho_0$–$5\rho_0$, the hybrid stars belong to the third family of compact stars. When the value of ρ_t is increased to $6\rho_0$, the hybrid stars with a CFL quark matter core become stable only for $\Delta \geq 125$ MeV. We get the masses for such hybrid stars in the range of 1.0–$2.1M_\odot$ with radii 9.3–13.5 km.

For comparison, in Figs. 4–6 we plot contours (dot-dashed/maroon lines) in the mass-radius plane, which are deduced with 90% confidence, by fitting the high quality spectra from the compact star X7 in the globular cluster 47 Tucanae [50]. These spectra were fitted within an improved hydrogen atmosphere model, which also accounts for the variations in the surface gravity with mass and radius of the compact stars. These $M - R$ contours indicate that a compact star with canonical mass $1.4M_\odot$ should have a radius in the range of ~13–17 km, whereas a compact star with canonical radius 10 km has a mass $\sim 2M_\odot$. The compact stars composed of only hadronic matter can satisfy either the constraint on the radius at the canonical mass or the constraint on the mass at the canonical radius [50]. Our results for the $\Delta = 50$–75 MeV with $\rho_t = 4\rho_0$–$5\rho_0$ are bounded by the dot-dashed maroon contours over a broad range of masses and radii. For these cases, compact stars with canonical mass $1.4M_\odot$ have radii 13.5 km and are composed of only hadronic matter. But, compact stars with radii around the canonical value 10 km have masses close to $2M_\odot$ and are hybrid stars with a CFL quark matter core. We also plot the $M - R$ curves obtained using the constraints imposed by the discoveries of the kHz quasiperiodic oscillations (QPOs) [51] and the x-ray transient XTE J1739-285 [52]. The frequency of the innermost stable circular orbit (ISCO) inferred from the QPOs limits the mass of the nonrotating compact stars to be

$$M \leq \frac{2200 \text{ Hz}}{\nu_{\text{ISCO}}} M_\odot. \tag{20}$$

The values of ν_{ISCO} are in the range of 1220–1310 Hz. The compact star radius must be smaller than the ISCO, which implies [51]

$$R \leq \frac{19\,500 \text{ Hz}}{\nu_{\text{ISCO}}} \text{ km}. \tag{21}$$

Radii limits for masses less than the upper limit scale with $M^{1/3}$. The discovery of XTE J1739-285 suggests that it contains a compact star rotating at 1122 Hz. This imposes the constraint on the maximum radius of a nonrotating compact star with mass M [53],

$$R_{\text{max}} \leq 9.63 \left(\frac{M}{M_\odot}\right)^{1/3}. \tag{22}$$

We see that the hybrid stars with $M \geq 1.4M_\odot$ satisfy the constraint as expressed by Eq. (22). It is also found in Refs. [54,55] that the mass of the compact star rotating with 1122 Hz is equal to or larger than $1.4M_\odot$.

In Table I we give the values of the maximum masses with corresponding central energy densities and radii for the hadronic and the hybrid stars obtained using different values of the Δ and ρ_t. It may be noted that, for a given Δ and ρ_t, the central energy density for the maximum mass of the hadronic star corresponds to the one at which the onset of the mixed phase occurs (see also Fig. 1). The values of maximum mass 1.7–$2.1M_\odot$ for the hybrid stars are consistent with the currently measured maximum mass $1.76 \pm 0.20M_\odot$ of PSR J0437-4715 [56] obtained by the precise determination of the orbital inclination angle. We note that, for $\rho_t = 5\rho_0$, the maximum mass of the hybrid stars with a CFL core are nearly equal to their second-family counterpart composed of hadrons. The hybrid stars with a CFL core are smaller by about 30% compared to their second-family counterpart. Thus, the hybrid stars with a CFL core are expected to rotate significantly faster in comparison to the hadronic stars. We also remark that our results for the mass-radius relationship are somewhat similar to the ones obtained using the NJL-like model [34,35], for the hybrid stars composed of a CFL or CCS quark matter core.

B. Mass-shedding limit sequences

In Fig. 7 we plot the relationship between the mass and the circumferential equatorial radius R_{eq} for the mass-shedding limit sequences obtained for the EOSs corresponding to different values of Δ and ρ_t. The portions of the curves to the left of the solid circles represent the hybrid stars with a CFL core. The cross symbol (×) on

TABLE I. The maximum mass of hybrid stars with a CFL core and hadron stars in the static limit, and the corresponding central energy density and radius obtained for different values of the CFL gap parameter Δ and the deconfinement phase transition density ρ_t.

		Hadron stars			Hybrid stars		
ρ_t	Δ (MeV)	ϵ (10^{15} g/cm^3)	M $M_\odot$	R (km)	ϵ (10^{15} g/cm^3)	M $M_\odot$	R (km)
	50	0.721	1.63	13.49	2.716	2.12	10.57
$4\rho_0$	100	0.642	1.45	13.52	2.863	2.05	10.16
	150	0.512	1.04	13.48	3.244	1.97	9.42
	50	0.873	1.94	13.34	2.863	1.96	10.53
$5\rho_0$	100	0.808	1.83	13.42	3.072	1.89	10.10
	150	0.690	1.62	13.55	3.663	1.80	9.28
	50	1.032	2.10	13.15	...	...	...
$6\rho_0$	100	0.959	2.04	13.24	...	...	...
	150	0.850	1.88	13.38	4.071	1.69	9.30

the different curves marks the maximum mass of the hybrid star. For $\rho_t = 5\rho_0$ with $\Delta = 50$ and 75 MeV, the third family of compact stars with a CFL core disappears from the mass-shedding limit sequence, though they exist in the static sequence as can be seen from Fig. 5. A similar situation is encountered for $\Delta \geq 125$ MeV with $\rho_t = 6\rho_0$ (see also Fig. 6). In Table II, we give the values of the central energy density, radius, and Kepler (mass-shedding) frequency f_K at the maximum mass for the hadronic and hybrid stars corresponding to different Δ and ρ_t. The values of the Keplerian frequency at the maximum hybrid star mass are in the range of 1.7–2 kHz, whereas the Keplerian frequency at the maximum mass for the hadronic stars is $\sim$1 kHz.

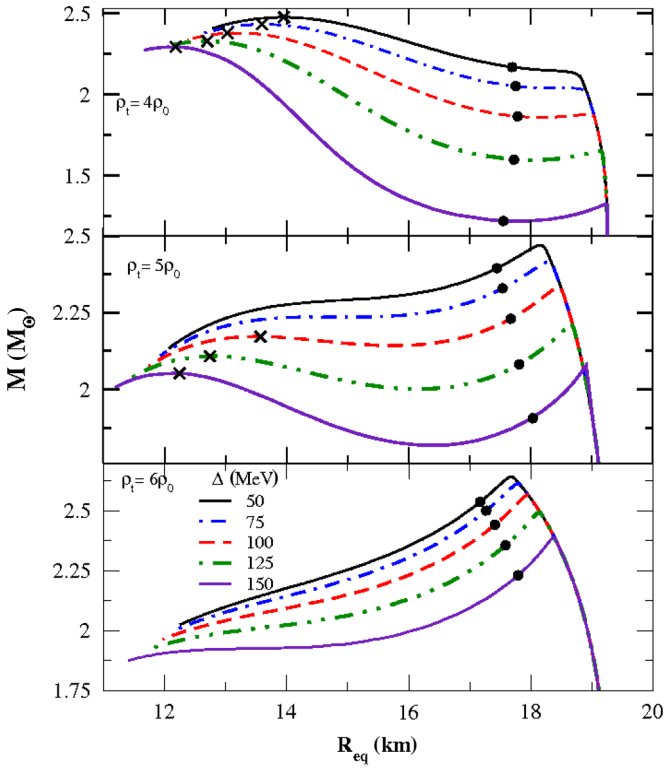

FIG. 7 (color online). Relationship between the mass M and the circumferential equatorial radius $R_{\rm eq}$ for mass-shedding limit sequences for different values of the CFL gap parameter and the phase transition densities $4\rho_0$ (upper panel), $5\rho_0$ (middle panel), and $6\rho_0$ (lower panel). The curves to the left of the solid circles represent the hybrid stars with a CFL core. The cross symbol ($\times$) on the different curves marks the maximum mass of the hybrid star.

We now examine several cases for which the third family of compact stars with a CFL core appears in the static sequence, but disappears from the mass-shedding limit sequence. We observe that, for these cases, the maximum mass of the third family of compact stars is lower than their second-family counterpart. In Fig. 8, we have plotted the mass-shedding limit sequences (upper panel) and the static sequences (lower panel) for $\Delta = 150$ MeV with ρ_t ranging from $5\rho_0$ to $6\rho_0$. We clearly see that the third family of compact stars tends to disappear beyond $\rho_t > 5.5\rho_0$. Strikingly, at $\rho_t = 5.5\rho_0$, the maximum masses of the second and third families of compact stars are nearly equal in the static limit. We find a similar outcome for the other cases (not shown here). Thus, it seems there exists a critical value of ρ_t for a given Δ beyond which the third family of compact stars with a CFL core tends to disappear with an increase in ρ_t. Below the critical value of ρ_t, such hybrid stars in the nonrotating limit have maximum mass higher than their counterpart composed of hadronic matter. These results are substantiated by the earlier calculations performed using different EOSs [34,57,58]. The EOS used in Ref. [34] yields a third family of compact stars in the static as well as in the mass-shedding limit sequences. For this EOS, the maximum mass of the compact star belonging to the third family is larger by about $0.1M_\odot$ compared to its second-family counterpart. On the other hand, for the EOSs used in Refs. [57,58], the third family of compact stars exists in the static limit and disappears from the mass-shedding limit sequences. For these EOSs, the maximum masses of the second and third families of compact stars are nearly equal. In Ref. [57], the maximum masses for the second and third families of compact stars are found to be $1.57M_\odot$

TABLE II. The central energy density, radius, and Kepler frequency at the maximum mass for the hybrid stars with a CFL core and hadron stars obtained for different values of the CFL gap parameter Δ and the deconfinement phase transition density ρ_t.

		Hadron stars				Hybrid stars			
ρ_t	Δ (MeV)	ϵ (10^{15} g/cm^3)	M $M_\odot$	R (km)	f_K (Hz)	ϵ (10^{15} g/cm^3)	M $M_\odot$	R (km)	f_K (Hz)
	50	0.721	2.09	18.84	1028	2.383	2.48	13.95	1698
$4\rho_0$	100	0.642	1.84	19.06	953	2.665	2.38	13.21	1803
	150	0.512	1.32	19.24	801	2.934	2.29	12.18	1993
	50	0.873	2.45	18.25	1158	...	...	...	...
$5\rho_0$	100	0.808	2.32	18.51	1107	2.842	2.17	13.44	1687
	150	0.690	2.08	18.95	1019	3.339	2.05	12.20	1889

and $1.55M_\odot$, respectively. In Ref. [58], the maximum masses for the second and third families of compact stars are $1.36M_\odot$ and $1.38M_\odot$, respectively.

C. Critical rotation frequency

We have computed the values of the maximum, or critical, rotation frequency $f_{\rm crit}$ for the stable configurations of hybrid stars with a CFL core. The stable configurations of the compact stars rotating at a given frequency f satisfy

$$\left(\frac{\partial M}{\partial \epsilon_c}\right)_f > 0. \tag{23}$$

Equation (23) is satisfied only for $f \leq f_{\rm crit}$. To locate the critical frequency we first obtained the variation in the mass as a function of ϵ_c at fixed frequencies in steps of 50 Hz. Then, for an appropriate interval of the frequency, the calculations were repeated by varying the frequency in steps of 5 Hz to determine the value of $f_{\rm crit}$. In Figs. 9 and 10 we plot the $M - R_{\rm eq}$ curves at fixed values of the rotational frequency. The black solid lines represent the results obtained at $f = f_{\rm crit}$. For clarity, we mainly focus on the regions of the $M - R_{\rm eq}$ curves corresponding to the sequences of the hybrid stars which are relevant in the present context. In this region, the value of $R_{\rm eq}$ decreases with an increase in ϵ_c. The results presented in Fig. 9

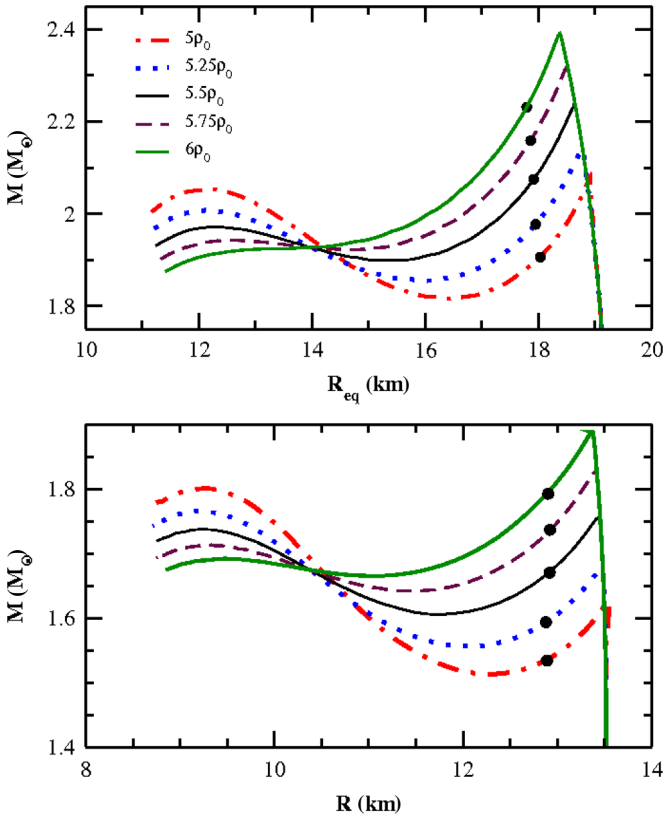

FIG. 8 (color online). Plots for the mass-shedding limit sequences (upper panel) and the static sequences (lower panel) for the CFL gap parameter $\Delta = 150$ MeV with a deconfinement phase transition density $\rho_t = 5\rho_0$–$6\rho_0$. The parts of the curves to the left of the solid circles in the upper and lower panels represent the sequences of hybrid stars with a CFL quark matter core.

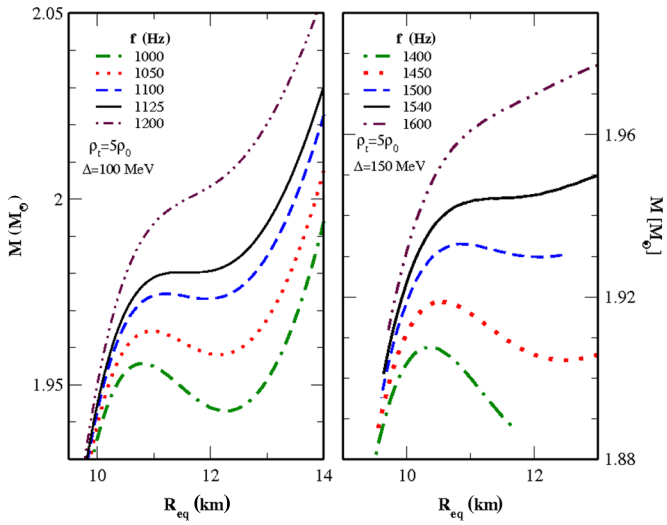

FIG. 9 (color online). Plots for the mass vs the circumferential equatorial radius $R_{\rm eq}$ at fixed values of the rotational frequency. The black solid lines represent the results obtained at the critical frequencies $f_{\rm crit}$. For $f > f_{\rm crit}$, third families of compact stars do not exist. The values of ρ_t and Δ considered are such that they yield a third family of compact stars in the static as well as in the mass-shedding limit sequences.

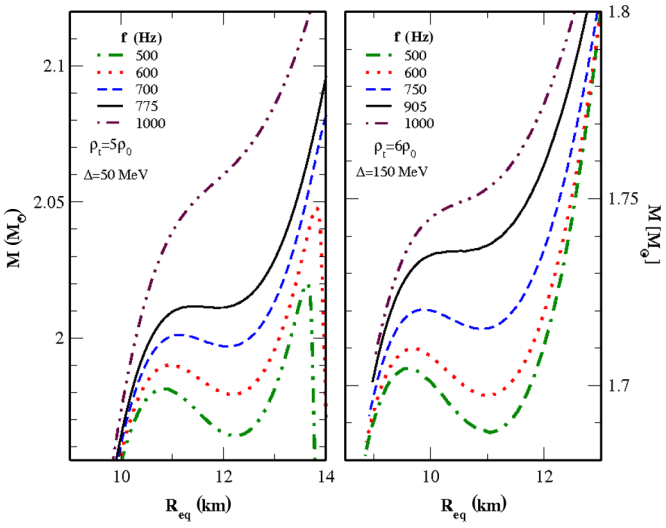

FIG. 10 (color online). Same as Fig. 9, but the values of ρ_t and Δ considered are such that they yield a third family of compact stars in the static sequences which disappears from the mass-shedding limit sequences.

correspond to the cases for which a third family of compact stars exists in the static as well as in the mass-shedding limit sequences. In Fig. 10, we consider the cases for which a third family of compact stars exists in the static limit but disappears from the mass-shedding limit sequences. We see that the value of $f_{\rm crit}$, for the cases presented in Fig. 9, are larger than the highest observed rotation frequency 1122 Hz. The value of $f_{\rm crit} \simeq 775$–900 Hz for the cases presented in Fig. 10. For $\rho_t = 4\rho_0$, the value of $f_{\rm crit}$ increases from 1370 Hz to 1805 Hz as the CFL gap parameter Δ increases from 50 MeV to 150 MeV. It may be pointed out that the situation analogous to that of Fig. 10 is encountered in Refs. [57,58], but the value of $f_{\rm crit}$ is about 350–650 Hz.

In Table III, we summarize the properties at the maximum mass of the hybrid stars with a CFL core rotating with critical frequency. We compare the values of $\epsilon_c(f_{\rm crit})$ as given in this table with the maximum $[\epsilon_c(0)]$ and the minimum $[\epsilon_c'(0)]$ energy densities at the center of stable configurations of nonrotating hybrid stars. In the last two columns of Table III we give the values of $\partial\epsilon_1$ and $\partial\epsilon_2$, calculated as

$$\partial\epsilon_1 = 1 - \frac{\epsilon_c(f_{\rm crit})}{\epsilon_c(0)} \tag{24}$$

and

$$\partial\epsilon_2 = 1 - \frac{\epsilon_c'(0)}{\epsilon_c(0)}. \tag{25}$$

The values of $\epsilon_c(0)$ and $\epsilon_c(f_{\rm crit})$ are taken from the sixth and fourth columns of Tables I and III, respectively. It is clear from the values of $\partial\epsilon_1$ that the central energy density $\epsilon_c(f_{\rm crit})$ is smaller than $\epsilon_c(0)$ by 25%–30%. The values of $\partial\epsilon_2$ are noticeably larger for the cases considered in Fig. 9 than those of Fig. 10. For $\rho_t = 4\rho_0$ with $\Delta = 150$ MeV, we get $\partial\epsilon_1 = 0.25$ and $\partial\epsilon_2 = 0.62$. We would like to add that the EOS used in Ref. [58] yields $\partial\epsilon_2 \simeq 0.4$, for which a third family of compact stars disappears from the mass-shedding limit sequence but exists in the static limit. It thus appears that $\partial\epsilon_2 \lesssim 0.4$ disfavors the appearance of a third family of compact stars in the mass-shedding limit sequence even if it exists in the static limit. It may be noted that the values of $f_{\rm crit}$ (Table III) are lower than the Kepler frequency (Table II) for the cases considered in Fig. 9. We would like to point out that the value of $f_{\rm crit}$ for a given EOS represents the maximum rotation frequency for which the stability condition as given by Eq. (23) is satisfied, whereas the mass-shedding limit sequences cannot be subjected to Eq. (23). Along these sequences, the rotation frequency corresponds to the Kepler frequency which increases with the central energy density. This leads to values of the Kepler frequency at a maximum mass higher than the $f_{\rm crit}$ for a given EOS.

IV. CONCLUSIONS

We construct static and mass-shedding limit sequences of hybrid stars for a set of EOSs obtained for different values of the CFL gap parameter and the deconfinement phase transition density. The hybrid stars considered are composed of CFL quark matter at the core, nuclear matter at the crust, and a mixed phase in the intermediate region. The hadronic part of the EOS is obtained using an appropriately calibrated, extended field theoretical based, relativistic mean-field model. The EOSs of quark matter in the CFL phase corresponding to different values of the CFL gap parameter and the deconfinement phase transition density are obtained using the MIT bag model with an

TABLE III. Properties at the maximum mass of hybrid stars with a CFL core rotating at the critical frequency as obtained for different values of the CFL gap parameter Δ and the deconfinement phase transition density ρ_t. The values of $\partial\epsilon_1$ and $\partial\epsilon_2$ are obtained using Eqs. (24) and (25).

ρ_t	Δ (MeV)	$f_{\rm crit}$ (Hz)	ϵ (10^{15} g/cm^3)	M ($M_\odot$)	$R_{\rm eq}$ (km)	$\partial\epsilon_1$	$\partial\epsilon_2$
	50	775	2.160	2.01	11.58	0.25	0.35
$5\rho_0$	100	1125	2.205	1.98	11.49	0.28	0.45
	150	1540	2.685	1.94	11.30	0.27	0.55
$6\rho_0$	150	905	2.951	1.74	10.62	0.28	0.30

additional parameter that mimics the effect of including perturbative QCD corrections. The CFL gap parameter ranges from 50–150 MeV, with the deconfinement phase transition density ranging from $4\rho_0$–$6\rho_0$ ($\rho_0 = 0.16$ fm^{-3}).

We find the existence of stable configurations of static hybrid stars for all the different values of the CFL gap parameter considered with the deconfinement phase transition density $4\rho_0$–$5\rho_0$. For the cases with CFL gap parameters in the range 50–100 MeV with a deconfinement phase transition density $4\rho_0$, the sequences of stable configurations of hybrid stars bifurcate from the hadronic sequence when the central density exceeds the one at which the onset of the mixed phase occurs. In all the other cases, the stable configurations of hybrid stars form the third family of compact stars. When the deconfinement phase transition density is increased to $6\rho_0$, the stable configurations of hybrid stars exist only for CFL gap parameters $\Delta \geq 125$ MeV. For the CFL gap parameters in the range 50–75 MeV with deconfinement phase transition density $4\rho_0$–$5\rho_0$, the mass-radius relationship over a broad range of masses and radii is in harmony with those deduced by applying an improved hydrogen atmosphere model to fit the high quality spectra from compact star X7 in the globular cluster 47 Tucanae. The values of the maximum mass 1.7–2.1$M_\odot$ for the hybrid stars are consistent with the currently measured maximum mass $1.76 \pm 0.20 M_\odot$ of PSR J0437-4715 [56].

We find for several cases that the third family of compact stars disappears from the mass-shedding limit sequences, though they appear in the corresponding static sequences. Our investigation suggests that the third family of compact stars is more likely to appear in the mass-shedding limit sequence, provided they have a maximum mass in the static limit higher than their counterpart composed of pure hadronic matter. Further, we have calculated the quantity $\partial\epsilon_2$ [Eq. (25)] obtained using the minimum and the maximum values of the central energy densities for the stable configurations of the static hybrid stars. The values of $\partial\epsilon_2$ are less than 0.4 for the cases in which a third family of compact stars disappears from the mass-shedding limit sequences but exists in the static limit. Except for these cases, the values of the critical rotation frequency for the hybrid stars with a CFL core are larger than the highest observed frequency 1122 Hz. The relationship between the values of $\delta\epsilon_2$ and the disappearance of the third family of compact stars from the mass-shedding limit sequences as observed in the present work is only preliminary. To establish this relationship, more investigations must be carried out using a wide variety of EOSs.

[1] N. Itoh, Prog. Theor. Phys. **44**, 291 (1970).
[2] A. R. Bodmer, Phys. Rev. D **4**, 1601 (1971).
[3] E. Witten, Phys. Rev. D **30**, 272 (1984).
[4] D. Bailin and A. Love, Phys. Rep. **107**, 325 (1984).
[5] M. G. Alford, Annu. Rev. Nucl. Part. Sci. **51**, 131 (2001).
[6] J. Bardeen, L. N. Cooper, and J. R. Schrieffer, Phys. Rev. **106**, 162 (1957).
[7] J. Bardeen, L. N. Cooper, and J. R. Schrieffer, Phys. Rev. **108**, 1175 (1957).
[8] M. G. Alford, K. Rajagopal, and F. Wilczek, Phys. Lett. B **422**, 247 (1998).
[9] S. B. Rüster and D. H. Rischke, Phys. Rev. D **69**, 045011 (2004).
[10] S. B. Rüster, V. Werth, M. Buballa, I. A. Shovkovy, and D. H. Rischke, Phys. Rev. D **72**, 034004 (2005).
[11] M. G. Alford, K. Rajagopal, and F. Wilczek, Nucl. Phys. **B537**, 443 (1999).
[12] K. Rajagopal and F. Wilczek, Phys. Rev. Lett. **86**, 3492 (2001).
[13] M. G. Alford, J. Bowers, and K. Rajagopal, Phys. Rev. D **63**, 074016 (2001).
[14] K. Rajagopal and R. Sharma, Phys. Rev. D **74**, 094019 (2006).
[15] N. D. Ippolito, M. Nardulli, and M. Ruggieri, J. High Energy Phys. 04 (2007) 036.
[16] V. R. Pandharipande and R. A. Smith, Nucl. Phys. **A237**, 507 (1975).
[17] E. Chabanat, P. Bonche, P. Haensel, J. Meyer, and R. Schaeffer, Nucl. Phys. **A627**, 710 (1997).
[18] J. R. Stone, J. C. Miller, R. Koncewicz, P. D. Stevenson, and M. R. Strayer, Phys. Rev. C **68**, 034324 (2003).
[19] L. Monras, Eur. Phys. J. A **24**, 293 (2005).
[20] B. K. Agrawal, S. K. Dhiman, and R. Kumar, Phys. Rev. C **73**, 034319 (2006).
[21] M. Prakash, J. R. Cooke, and J. M. Lattimer, Phys. Rev. D **52**, 661 (1995).
[22] N. K. Glendenning and J. Schaffner-Bielich, Phys. Rev. C **60**, 025803 (1999).
[23] A. W. Steiner, M. Prakash, J. M. Lattimer, and P. Ellis, Phys. Rep. **411**, 325 (2005).
[24] H. Müther, M. Prakash, and T. L. Ainsworth, Phys. Lett. B **199**, 469 (1987).
[25] L. Engvik, M. Hjorth-Jensen, E. Osnes, G. Bao, and E. Østgaard, Phys. Rev. Lett. **73**, 2650 (1994).
[26] L. Engvik, E. Osnes, M. Hjorth-Jensen, G. Bao, and E. Østgaard, Astrophys. J. **469**, 794 (1996).
[27] H. J. Schulze, A. Polls, A. Ramos, and I. Vidana, Phys. Rev. C **73**, 058801 (2006).
[28] M. Alford and S. Reddy, Phys. Rev. D **67**, 074024 (2003).
[29] S. Banik and D. Bandyopadhyay, Phys. Rev. D **67**, 123003 (2003).
[30] M. Alford, Prog. Theor. Phys. Suppl. **153**, 1 (2004).
[31] M. Baldo, M. Buballa, F. Burgio, F. Neumann, M. Oertel, and H. Schulze, Phys. Lett. B **562**, 153 (2003).

[32] M. Buballa, Phys. Rep. **407**, 205 (2005).
[33] T. Klähn, D. Blaschke, F. Sandin, C. Fuchs, A. Faessler, H. Grigorian, G. Ropke, and J. Trümper, Phys. Lett. B **654**, 170 (2007).
[34] N. D. Ippolito, M. Ruggieri, D. H. Rischke, A. Sedrakian, and F. Weber, Phys. Rev. D **77**, 023004 (2008).
[35] G. Pagliara and J. Schaffner-Bielich, Phys. Rev. D **77**, 063004 (2008).
[36] J. W. Negele and D. Vautherin, Nucl. Phys. **A207**, 298 (1973).
[37] G. Baym, C. Pethick, and P. Sutherland, Astrophys. J. **170**, 299 (1971).
[38] R. Furnstahl, Nucl. Phys. **A706**, 85 (2002).
[39] T. Sil, M. Centelles, X. Vinas, and J. Piekarewicz, Phys. Rev. C **71**, 045502 (2005).
[40] S. K. Dhiman, R. Kumar, and B. K. Agrawal, Phys. Rev. C **76**, 045801 (2007).
[41] H. Müller and B. D. Serot, Nucl. Phys. **A606**, 508 (1996).
[42] M. Alford, M. Braby, M. Paris, and S. Reddy, Astrophys. J. **629**, 969 (2005).
[43] E. S. Fraga, R. D. Pisarski, and J. Schaffner-Bielich, Phys. Rev. D **63**, 121702 (2001).
[44] D. T. Son and M. A. Stephanov, Phys. Rev. D **61**, 074012 (2000).
[45] N. K. Glendenning, *Compact Stars: Nuclear Physics, Particle Physics, and General Relativity* (Springer-Verlag, New York, 2000).
[46] P. K. Panda and H. S. Nataraj, Phys. Rev. C **73**, 025807 (2006).
[47] R. Rapp, T. Schäfer, E. Shuryak, and M. Velkovsky, Phys. Rev. Lett. **81**, 53 (1998).
[48] N. Stergioulas and J. L. Friedman, Astrophys. J. **444**, 306 (1995).
[49] J. Schaffner-Bielich and A. Gal, Phys. Rev. C **62**, 034311 (2000).
[50] C. O. Heinke, G. B. Rybicki, R. Narayan, and J. E. Grindlay, Astrophys. J. **644**, 1090 (2006).
[51] M. C. Miller, F. K. Lamb, and D. Psaltis, Astrophys. J. **508**, 791 (1998).
[52] P. Kaaret, Z. Prieskorn, J. J. M. in 't Zand, S. Brandt, N. Lund, S. Mereghetti, D. Gotz, E. Kuulkers, and J. Tomsick, Astrophys. J. **657**, L97 (2007).
[53] J. M. Lattimer and M. Prakesh, Phys. Rep. **442**, 109 (2007).
[54] M. Bejger, P. Haensel, and J. L. Zdunik, Astron. Astrophys. **464**, L49 (2007).
[55] P. Haensel, J. L. Zdunik, and M. Bejger, New Astron. Rev. **51**, 785 (2008).
[56] J. P. W. Verbiest, M. Bailes, W. van Straten, G. B. Hobbs, R. T. Edwards, R. N. Manchester, N. D. R. Bhat, J. M. Sarkissian, B. A. Jacoby, and S. R. Kulkarni, Astrophys. J. **679**, 675 (2008).
[57] S. Banik, M. Hanauske, and D. Bandyopadhyay, J. Phys. G **31**, S841 (2005).
[58] A. Bhattacharyya, S. K. Ghosh, M. Hanauske, and S. Raha, Phys. Rev. C **71**, 048801 (2005).